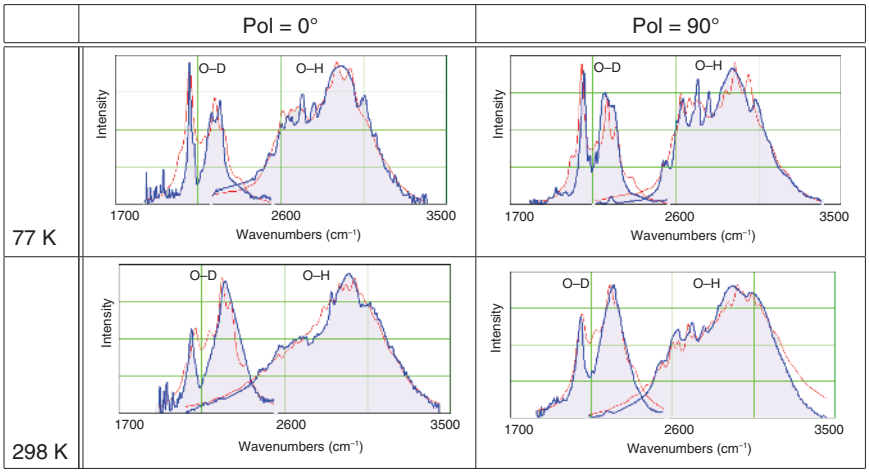

Figure 1.14 Temperature and isotopic substitution effects at different polarizations for crystalline glutaric acid with Fermi resonances. Grayed: Experimental lineshapes of Flakus and Miros [24]. Source: Based on Flakus and Miros [24].

Table 1.9a Parameters used for fitting the experimental lineshapes of crystalline glutaric in presence of Fermi resonance, given in Figure 1.14.

Pol (°)	Case	T (K)	$\omega°(\text{cm}^{-1})$	Ω (cm^{-1})	$\alpha°$	$\gamma°(\Omega)$	$\gamma(\Omega)$	$V°(\Omega)$	$\eta°$
	O–H	77	3063	90	1.50	0.20	0.10	−115	0.55
0	O–H	298	3063	90	1.50	0.15	0.20	−1.15	0.12
	O–D	77	2202	90	0.38	0.15	0.20	−0.82	1.00
	O–D	298	2217	90	0.38	0.10	0.20	−0.82	0.40
	O–H	77	3083	90	1.50	0.20	0.20	−1.15	0.70
0	O–D	298	3083	90	1.50	0.25	0.25	−1.15	0.40
	O–H	77	2188	90	0.38	0.20	0.20	-0.82	1.00
	O–D	298	2217	90	0.38	0.25	0.25	−0.82	0.50

The line shapes were studied within the frameworks of our original theory of strong anharmonic coupling, Davydov coupling, Fermi resonance coupling, direct and indirect damping, and a selection rule breaking mechanism for forbidden transitions in IR.

The present approach (see Figure 1.17) correctly fits the experimental line shape of the hydrogenated compound and predicts satisfactorily the evolution in the lineshapes with isotopic substitution. Numerical calculations show that mixing of all these effects allows one to reproduce satisfactorily the main features of the experimental IR lineshapes of hydrogenated and deuterated 2-NA crystals and is expected to confirm the importance of the Fermi resonances in reproducing the experimental spectra. Parameters are given in Tables 1.12 and 1.13.

Table 1.9b (continued). Fermi resonances parameters for crystalline glutaric acid (cf. Figure 1.14).

Pol	Case	T (K)	$f_1^{\bar{\nu}}$	$f_2^{\bar{\nu}}$	$f_3^{\bar{\nu}}$	$f_4^{\bar{\nu}}$	$f_5^{\bar{\nu}}$	$\Delta_1^{\bar{\nu}}$	$\Delta_2^{\bar{\nu}}$	$\Delta_3^{\bar{\nu}}$	$\Delta_4^{\bar{\nu}}$	$\Delta_5^{\bar{\nu}}$	$\gamma_1^{\bar{\nu}}$	$\gamma_2^{\bar{\nu}}$	$\gamma_3^{\bar{\nu}}$	$\gamma_4^{\bar{\nu}}$	$\gamma_5^{\bar{\nu}}$
			(cm^{-1})	(cm^{-1})	(cm^{-1})	(cm^{-1})	(cm^{-1})	(cm^{-1})	(cm^{-1})	(cm^{-1})	(cm^{-1})	(cm^{-1})	(Ω)	(Ω)	(Ω)	(Ω)	(Ω)
	O–H	77															
0	O–H	298	40	25	20	30	30	−430	−120	30	100	200	0.10	0.10	0.10	0.10	0.10
	O–D	77															
	O–D	298															
	O–H	77		23									0.05	0.05	0.05	0.05	0.05
90	O–H	298	40	0	20	30	30	−430	−430	30	310	200	0.10	0.10	0 10	0.10	0.10
	O–D	77		25									0.10	0.10	0.10	0.10	0.10
	O–D	298		0									0.10	0.10	0.10	0.10	0.10

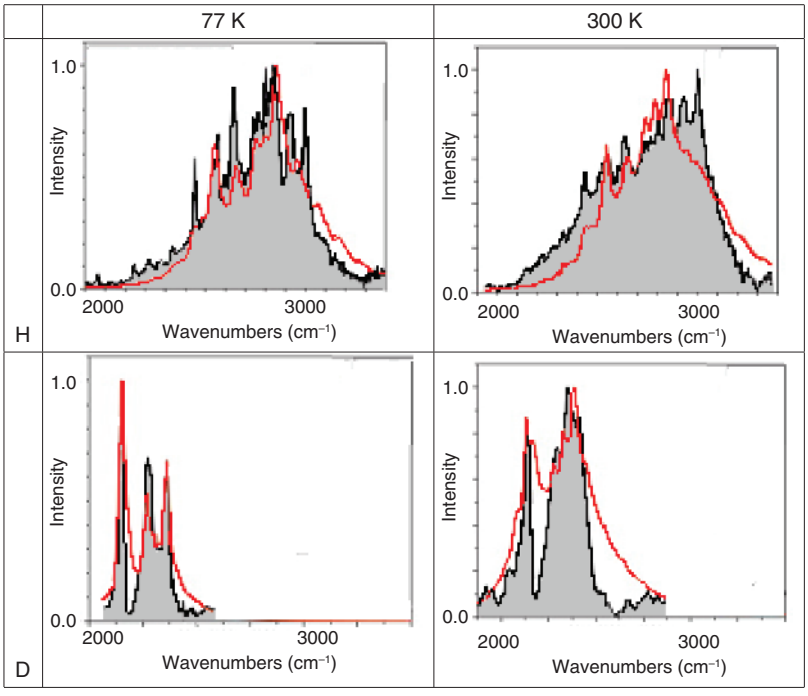

Figure 1.15 Crystalline H(D)-3-thiophenacrylic acid experimental (H-3TAcetic) (grayed) and theoretical lineshapes at different temperatures and H/D isotopic species. Source: Modified from Rekik et al. 2015 [31].

Table 1.10 Parameters used for fitting the experimental lineshapes of the 3-thiopheneacetic (H-3TAcetic) acid crystals dimers and their deuterated analogs (Pol = 0).

Species	T (K)	$\omega°(\text{cm}^{-1})$	$\Omega(\text{cm}^{-1})$	$\alpha°$	$\gamma°(\Omega)$	$\gamma(\Omega)$	$VD°(\Omega)$	Θ
H-3TAcetic	77	3180	105	1.55	0.35	0.35	0.50	0.15
H-3TAcetic	300	3050	105	1.2	0.3	0.25	1.2	0.22
D-3TAcetic	77	2250	80	0.67	0.15	0.25	0.52	0.2
D-3TAcetic	300	2250	85	0.63	0.17	0.25	0.7	0.2

1.3.2.5 Crystalline Aspirin Dimers Involving Slow Mode Morse Potential

The application of our treatment for Davydov coupling has been performed with aspirin by Rekik and coworkers [27] by accounting for the anharmonicity of the slow mode which is described by a "Morse" potential with a dissociation energy of $D_e = 2100\,\text{cm}^{-1}$ to reproduce the polarized IR spectra of the hydrogen and deuterium bond in acetylsalicylic acid (aspirin) crystals.

Within the adiabatic approximation, the Hamiltonian of each moiety of the dimer may be put on the form of sum of effective Hamiltonians which are depending on the degree of excitation of the fast mode.

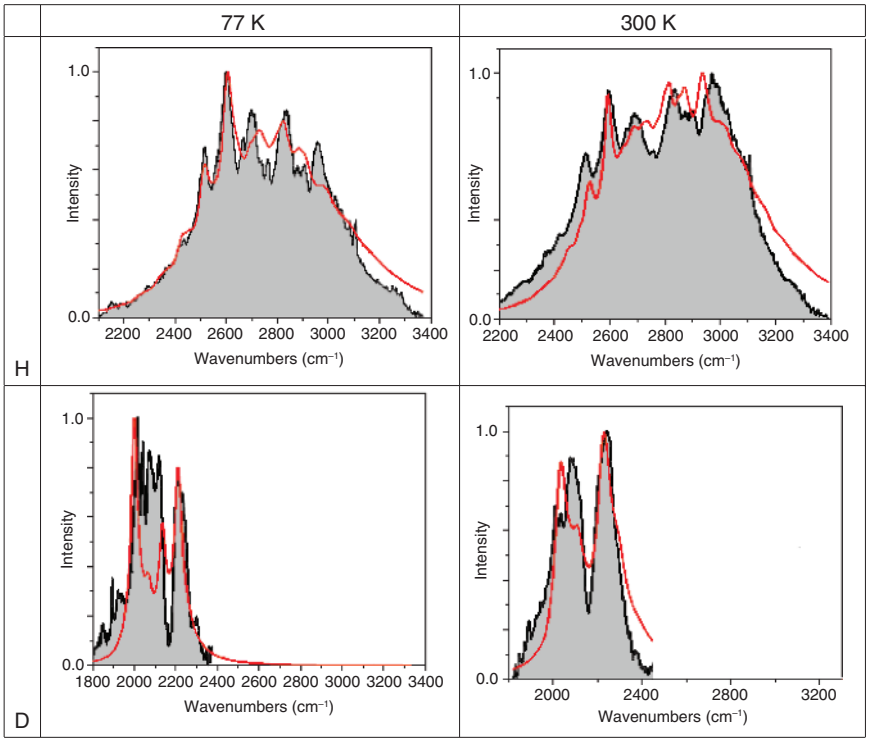

Figure 1.16 Crystalline H(D)-3-thiophenacrylic acid experimental (black line); theoretical (red line) lineshapes at different temperatures for H and D isotopic species. Source: Rekik et al. 2015 [31]/With permission of Elsevier.

Table 1.11 Parameters used for fitting the experimental lineshapes of the crystalline 3-thiopheneacrylic (H-3TAcrylic) acid dimers and their deuterated analogs.

Pol = 0	T (K)	$\omega°(\text{cm}^{-1})$	$\Omega(\text{cm}^{-1})$	$\alpha°$	$\gamma°(\Omega)$	$\gamma(\Omega)$	$VD°(\Omega)$	Θ
H-3TAcrylic	77	2950	85	1.1	0.3	0.3	0.9	0.23
H-3TAcrylic	300	3020	85	1.23	0.3	0.15	1	0.23
D-3TAcrylic	77	2125	75	0.65	0.22	0.2	0.65	0.12
D-3TAcrylic	300	2150	75	0.63	0.24	0.25	0.65	0.4

These corrections are introduced in the usual procedure for taking into account the Davydov coupling. The theoretical lineshapes obtained are compared to the experimental ones obtained by these authors for the two isotopic species at 77 and 300 K temperatures. Their results are given in Figure 1.18 and the coresponding parameters in Table 1.14.

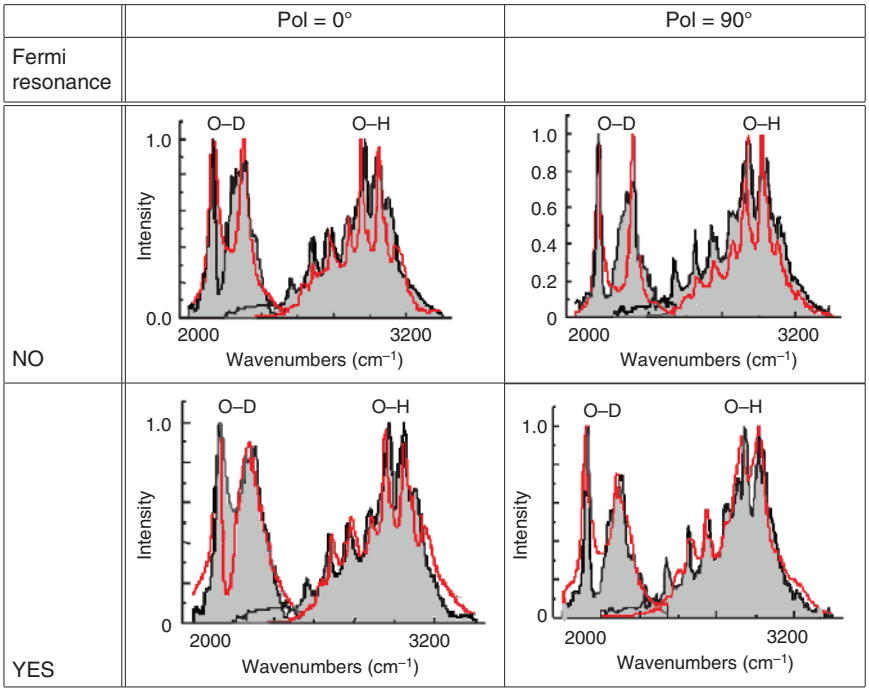

Figure 1.17 2-Naphtylacetic Acid (2-NA). Comparison of experimental lineshapes with theoretical ones for different polarizations and isotopic substitutions, without and with 3 Fermi resonances. Source: Issaoui et al. 2013 [26]/ Springer Nature.

Table 1.12 Parameters used to fit experimental H/D-2-NA spectra.

Species	Pol(°)	$\omega°\,(\mathrm{cm}^{-1})$	$\Omega\,(\mathrm{cm}^{-1})$	$\alpha°$	$\gamma°(\Omega)$	$\gamma(\Omega)$	$V°(\hbar\Omega)$	η
–H	0	3135	67	1.56	0.20	0.05	−1.55	0.45
–H	90	3110	65	1.60	0.22	0.002	−1.65	0.20
–D	0	2221	90	0.364	0.30	0.10	−0.857	0.98
–D	90	2221	90	0.364	0.17	0.10	−1.00	0.98

1.3.2.6 Phthalic and Terephthalic Acid Crystals

Phthalic (PAC) and terephthalic (TAC) acid crystals have been studied by Rekik et al. [36].

They have studied two interacting cyclic dimers shown in Figure 1.19 in which the q_i and Q_i are respectively the fast and slow modes position coordinates while $V°_{D_1}$ and $V°_{D_2}$ are the Davydov coupling involved in each system of the superdimer. They have considered the full Hamiltonian of the superdimer for its diagonal part as the

Table 1.13 Values of Fermi coupling parameters used for fitting experimental H/D-2-NA spectra.

Pol(°)	$f_1(\text{cm}^{-1})$	$f_2(\text{cm}^{-1})$	$f_3(\text{cm}^{-1})$	$\Delta_1(\text{cm}^{-1})$	$\Delta_2(\text{cm}^{-1})$	$\Delta_3(\text{cm}^{-1})$	$\gamma_{\Delta_1}(\Delta_1)$	$\gamma_{\Delta_2}(\Delta_2)$	$\gamma_{\Delta_3}(\Delta_3)$
–H 0	10	10	20	60	−80	42	0.4	0.4	10
–H 90	20	10	10	110	120	150	0.2	0.2	0.2
–D 0	20	30	30	140	110	−180	0.2	0.2	0.2
–D 90	20	30	30	140	110	−180	0.2	0.2	0.2

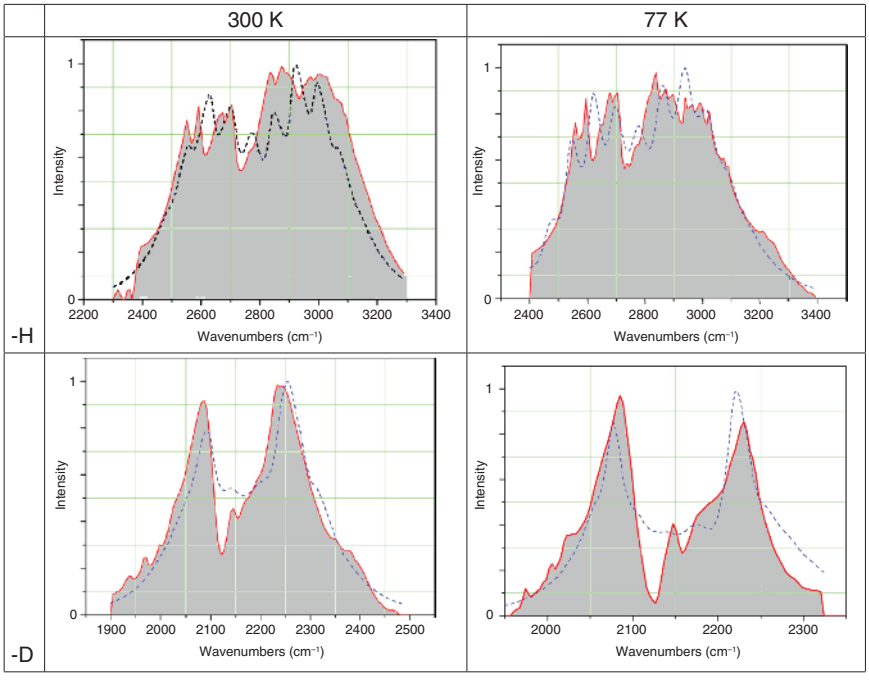

Figure 1.18 Comparison between the experimental (grayed) and theoretical (dashed line) spectra for Aspirin-H (polycrystalline acetylsalicylic acid) at 300 and 77 K. Source: Ghalla et al. 2010 [27]/ With permission of Elsevier.

Table 1.14 Parameters used for fitting experimental Aspirin-H and Aspirin-D acid dimer spectra.

Compound	T(K)	$\omega°(\text{cm}^{-1})$	$\Omega(\text{cm}^{-1})$	$\alpha°$	$V°$	$\gamma°(\Omega)$	$\gamma(\Omega)$	η
Aspirin-H	300	2910	76	0.95	−1.75	0.25	0.1	0.85
Aspirin-H	77	3095	77	1.62	−1.70	0.35	0.1	0.8
Aspirin-D	300	2185	86	0.743	−1.69	0.25	0.7	0.7
Aspirin-D	77	2228	77	1.238	−1.65	0.25	1.1	0.8

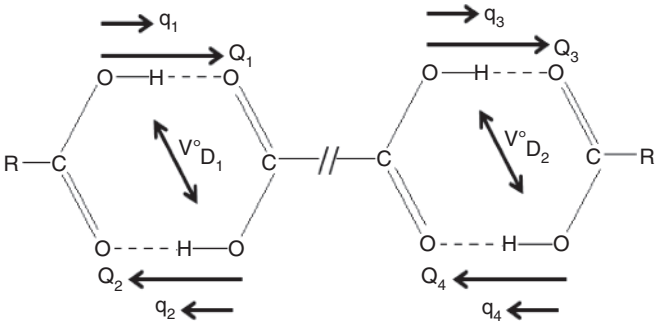

Figure 1.19 Structure of the superdimer and definition of the eight vibrational modes involved in the superdimer dynamics.

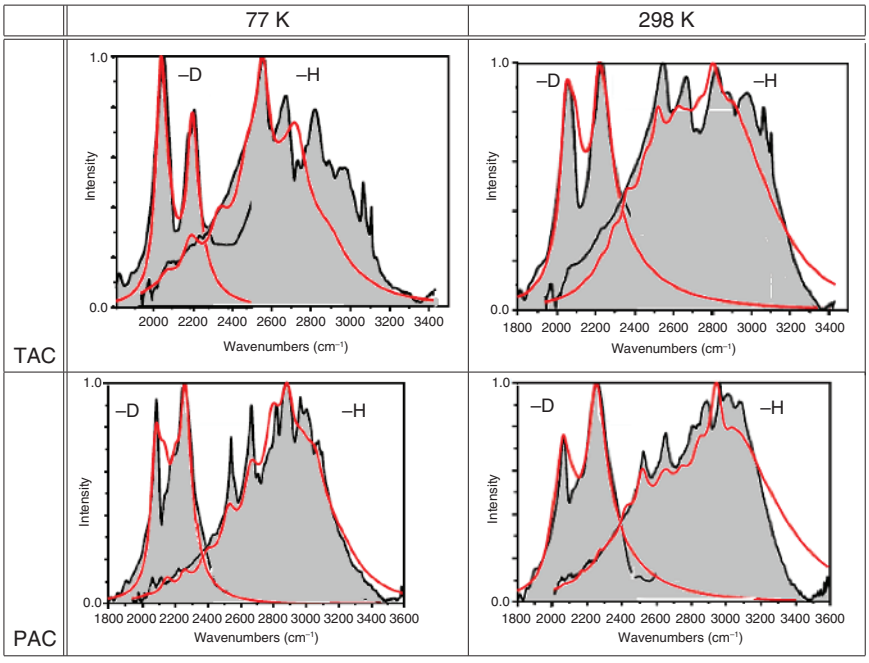

Figure 1.20 Crytalline phthalic (PAC) and terephthalic (TAC) acids at 77 and 298 K. Comparison of experimental (grayed) and theoretical (full line) lineshape. Source: Based on Rekik et al. 2020 [36].

sum of the diagonal parts of each component and as for its off parts as the sum of the Davydov couplings of each component. Their results are shown in Figure 1.20 for the H6 and D6 isotopomers of Phthalic (PAC) and terephthalic (TAC) acid crystals using the parameters given in Table 1.15.

1.3.2.7 Liquid Formic Acid Mixing of Monomer and Dimer

A full quantum-theoretical approach has been used by Fathi et al. [28] to study the mOAH experimental IR lineshapes of liquid formic acid. For this purpose, the

Table 1.15 Theoretical parameters used for the fitting of the experimental lineshapes of PAC and TAC.

Cases	T(K)	$\omega^{\circ}_{D_1}$ (cm^{-1})	$\alpha^{\circ}_{D_2}$ (cm^{-1})	Ω_{D_1} (cm^{-1})	Ω_{D_2} (cm^{-1})	α	κ	$\gamma^{\circ}(\omega^{\circ\circ}_{D_1})$	$V^{\circ}_{D_1}(\Omega_{D_1})$	$V^{\circ}_{D_2}(\Omega_{D_2})$
D6 PAC	77	2180	2193	69	62	0.85	0.95	0.32	0.84	0.8
D6 PAC	298	2150	2167	64	60	0.96	0.87	0.31	1.29	1.35
D6 TAC	77	2130	2142	70	66	1.15	1.04	0.27	1.76	1.8
D6 TAC	298	2130	2119	62	65	1.02	1.13	0.25	1.83	1.8
H6 PAC	77	3200	3188	68	61	1.26	1.36	0.37	0.68	0.6
H6 PAC	298	3050	3012	64	71	1.45	1.39	0.34	1.02	1.06
H6 TAC	77	2860	2895	66	68	1.49	1.57	0.24	1.06	1.10
H6 PTAC	298	2850	2887	63	65	1.52	1.48	0.28	1.46	1.41

Table 1.16 Parameters used in the theoretical fitting of formic acid species.

Species	ω°(cm^{-1})	Ω(cm^{-1})	α°	V°_{D}	$\gamma^{\circ}(\Omega)$	$\gamma(\Omega)$	η	r
HCOOH	3030	95	1.4	−1.2	0.5	0.1	0.0	0.25
HCOOD	2340	110	0.85	−1.0	0.5	0.1	0.3	0.12
DCOOH	3080	95	1.5	−1.2	0.7	0.03	0.1	0.15
DCOOD	2240	110	0.62	−0.75	0.3	0.02	0.08	0.25

authors use our original theory, based on the strong anharmonic coupling between the high-frequency mode and the H-bond bridge, and including the Davydov coupling between the excited states of the two moieties, multiple Fermi resonances between the mOAH (Bu) mode and combinations of some bending modes, together with the quantum direct and indirect dampings. They have studied the influence of the proportion of dimers species with respect to monomers to obtain the best fitting with experimental spectra. This model reproduces satisfactorily the main features of the experimental lineshapes of liquid hydrogenated and deuterated formic acid, by using a minimum set of independent parameters as it may be seen in Figure 1.21.

In Tables 1.16 and 1.17 are given the parameters used in the calculation. r is the ratio Dimer/Monomer. The other parameters are those used in our original theory.

Parameters used to reproduce the experimental spectra of HCOOH and its deuterated derivatives DCOOH, HCOOD, and DCOOD of Figure 1.21.

1.3.2.8 Crystalline Furoic Acid Dimer with Slow Mode Morse Potential and Fermi Resonances

Ghalla et al. [29], have compared the experimental IR lineshapes of polarized crystalline Furoic acid dimers [30] at 77 K with their theoretical ones calculated

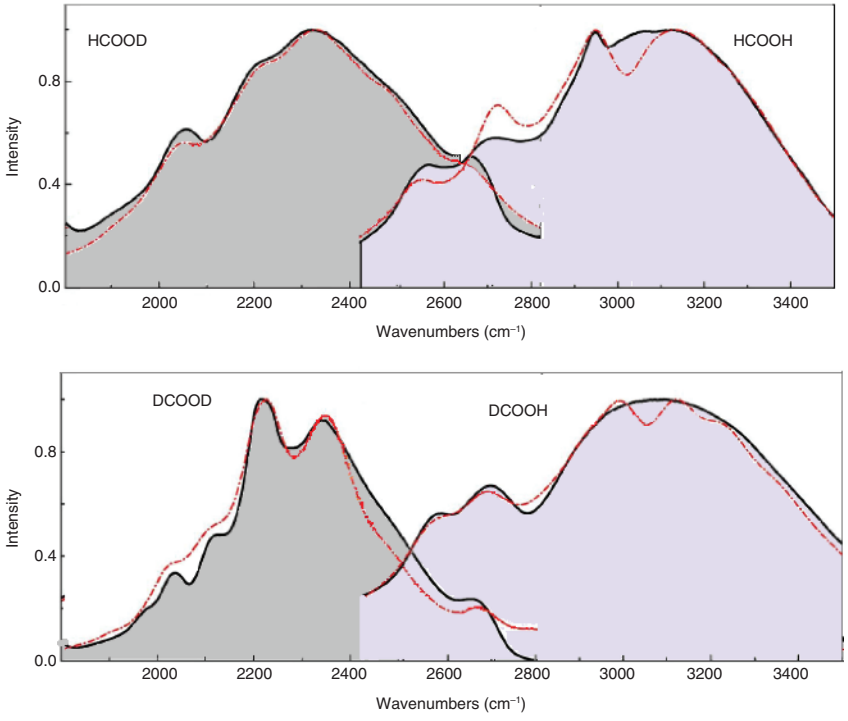

Figure 1.21 Liquid formic acid mixing of monomer and dimer of several H/D species. Experiment: grayed: Dashed red: theory. The corresponding parameters are given in Tables 1.16 and 1.17. Source: Modified from Fathi et al. 2017 [28].

Table 1.17 Fermi resonances parameters for crystalline glutaric acid (cf. Figure 1.14.

Species	f_1 (cm^{-1})	f_2 (cm^{-1})	f_3 (cm^{-1})	f_4 (cm^{-1})	ω_1 (cm^{-1})	ω_2 (cm^{-1})	ω_3 (cm^{-1})	ω_4 (cm^{-1})	γ_{δ_1} (Ω)	γ_{δ_1} (Ω)	γ_{δ_3} (Ω)	γ_{δ_4} (Ω)
HCO_2H	30	85	95	–	3130	2660	2850	–	0.1	0.05	0.02	–
HCO_2D	60	75	75	50	2285	2670	2110	2495	0.01	0.01	0.01	0.01
DCO_2H	–	75	135	–	–	2710	2850	–	–	0.01	0.01	–
DCO_2D	50	30	70	35	2060	2350	2680	2140	0.02	0.2	0.02	0.0

by introducing Morse potential for the slow modes. Their results are given in Figure 1.22.

They have improved the agreement with experiment by introducing in the model 3 Fermi resonances. In both situations, the theoretical lineshapes appear as continuous lines whereas the experimental ones are grayed.

In Figure 1.23 is given the comparison between the experiment (grayed) and theory as computed by Eq. (1.25). The slow modes are described by a Morse potential. The parameters used in the computations are given in Tables 1.18 and 1.19.

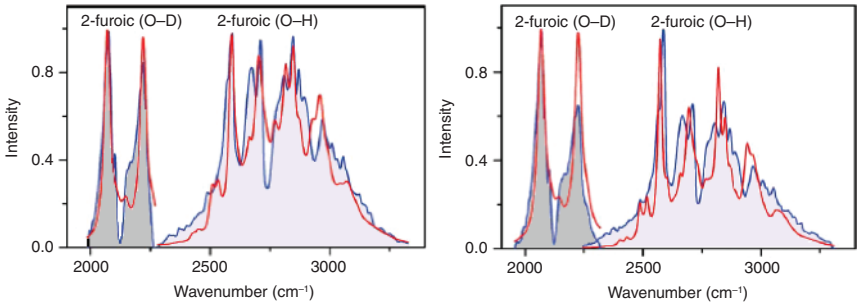

Figure 1.22 Lineshapes of polarized 2-furoic acid when the Fermi resonances are ignored, at 77 K. Source: Ghalla et al. [29]/John Wiley & Sons.

Table 1.18 Parameters involved for fitting the experimental spectra of 2-furoic acid.

Species	Pol(°)	$\omega°\,(\mathrm{cm}^{-1})$	$\Omega\,(\mathrm{cm}^{-1})$	$\alpha°$	$V°(\hbar\Omega)$	$\gamma°(\Omega)$	$\gamma(\Omega)$
H	0	3030	80	1.45	1.10	0.2	0.1
D	0	2142	90	0.331	0.786	0.15	0.1
H	90	2995	85	1.36	1.13	0.15	0.1
D	90	2144	87	0.318	0.857	0.18	0.1

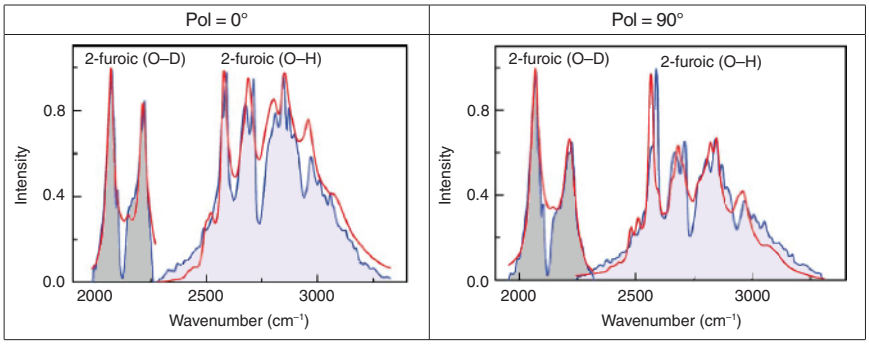

Figure 1.23 Lineshapes of polarized 2-furoic acid when there are three Fermi resonances at 77 K. Source: Ghalla et al. [29]/John Wiley & Sons.

Table 1.19 Fermi coupling parameters (in cm^{-1}) used for fitting experimental 2-furoic acid spectra.

	Pol(°)	$f_1(\mathrm{cm}^{-1})$	$f_2(\mathrm{cm}^{-1})$	$f_3(\mathrm{cm}^{-1})$	$\Delta_1(\mathrm{cm}^{-1})$	$\Delta_2(\mathrm{cm}^{-1})$	$\Delta_3(\mathrm{cm}^{-1})$	$\gamma_{\Delta_1}(\Delta_1)$	$\gamma_{\Delta_1}(\Delta_2)$	$\gamma_{\Delta_3}(\Delta_3)$
H	0	95	95	80	30	20	10	0.2	0.2	0.2
D	0	93	105	116	10	10	10	0.2	0.2	0.2
H	90	95	95	100	20	20	10	0.2	0.2	0.2
D	90	83.1	105	106	10	10	10	0.2	0.2	0.2

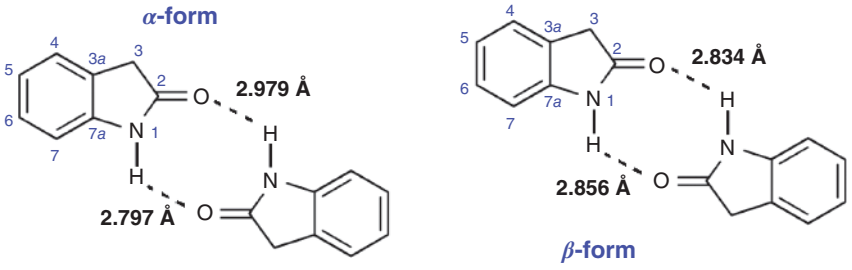

Figure 1.24 The two forms of oxindol.

Table 1.20 Parameters used for fitting the experimental line shapes of the ν_S(N–H) stretching band of (α/β)-hydrogenated and (α/β)-deuterated oxindole complexes at $T = 77$ K and $T = 293$ K.

Compound	T(K)	ω°_1 (cm^{-1})	ω°_2 (cm^{-1})	α_1	α_2	$\Omega_1 = \Omega_2$ (cm^{-1})	$\gamma^\circ(\Omega)$	$V^{HH/DD}_{Dav}$ (cm^{-1})
α-D oxindole	77	2350	2460	0.65	0.726	65	0.37	85.8
β-D oxindole	77	2352	2293	0.50	0.518	67	0.40	93.4
α-D oxindole	293	2350	2475	0.65	0.712	65	0.35	65
β-D oxindole	293	2280	2367	0.70	0.714	65	0.36	91
α- H oxindole	77	3160	3335	1.0	1.230	75	0.39	167.5
β-H oxindole	77	3070	3159	1.0	1.068	70	0.38	179
α-H oxindole	293	3110	3296	1.0	1.160	80	0.40	144
β-H oxindole	293	3120	3230	1.0	1.040	70	0.40	176

1.3.2.9 Other Kinds of H-Bonded Compounds

Combined Crystalline Oxindole Acid Dimers Another application was done by Ghalla et al. on oxindole crystals (2,3-dihydro-1*H*-indol-2-one) which form cyclic dimers with two different H-bonds [34]. In these molecules, we find the group H-N-C=O which is involved in the formation of cyclic dimer of H-bonds (α-form; β-form). They studies 2 forms of oxindol crystal, the α- and the β forms. The oxindole acid molecules form a cyclic, non-centrosymmetric acid dimer with two different H-bond bridges because they have different bond lengths as it is shown in Figure 1.24.

They have introduced for the coupling of the fast mode angular frequency with the slow mode coordinate of the hydogenated and deuterated compounds, a subtil dependence on the slow mode coordinate The consequence is that there are two different coupling parameters. Using the parameters of Table 1.20 the following spectra are given in Figure 1.25.

1.3.2.10 Phosphinic Acid Dimer

Hydrogen-bonded dimers of phosphinic acid (See Figure 1.26) and their deuterated analogs [($R_2POOH(D)$, with R = CH_2Cl, CH_3], IR lineshapes of phosphinic acids

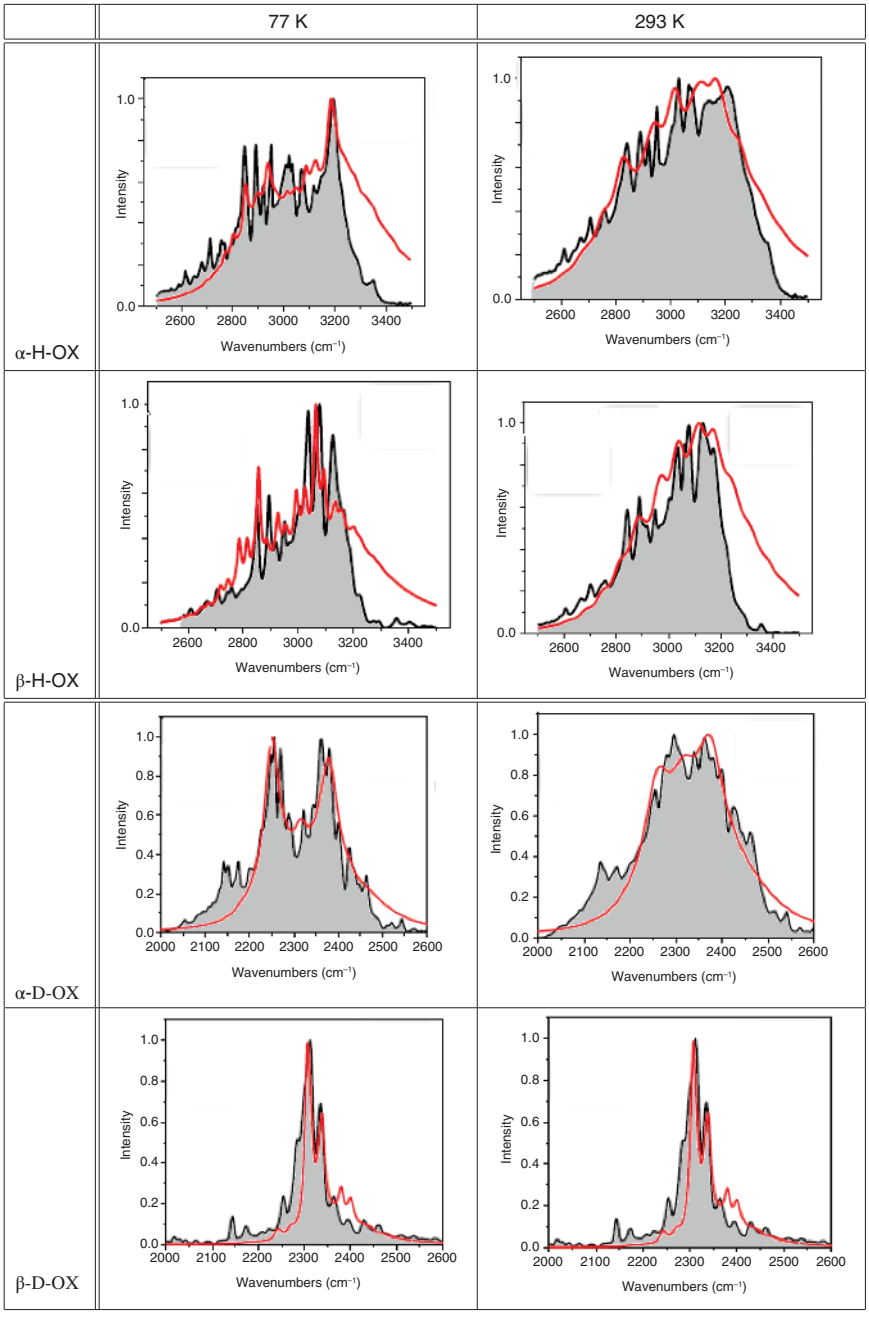

Figure 1.25 Lineshapes of (α/β)-hydrogenated and (α/β)-deuterated oxindole complexes at $T = 77$ K and $T = 293$ K. Grayed: experimental spectra. Source: Rekik et al. 2020 [36] / With permission of Elsevier.

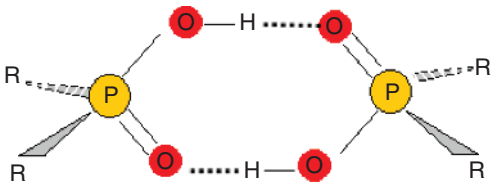

Figure 1.26 Dimer of phosphinic acid.

Table 1.21a Parameters used for fitting the experimental lineshapes of $(CH_2Cl)_2PO_2H/D$ and $(CH_3)_2PO_2H/D$.

	T(K)	$\omega°$(cm^{-1})	Ω(cm^{-1})	D_e(cm^{-1})	α	$\gamma°(\Omega)$	$\gamma(\Omega)$	$V_D(\Omega)$	η
$(CH_2Cl)_2PO_2H$	435	2300	205	2100	0.80	0.40	0.1	1.68	0.9
$(CH_2Cl)_2PO_2D$	475	1860	202	2100	0.25	0.35	0.1	0.55	0.49
$(CH_3)_2PO_2H$	530	2415	206	2100	0.95	0.55	0.1	1.9	0.6
$(CH_3)_2PO_2D$	515	1880	204	2100	0.30	0.65	0.1	0.78	0.29

R_2PO_2H dimers in the gas phase have been studied by Rekik and Alshammari [32] and compared with experiment [35] (See **Figure** 1.27)

The theoretical model is based on a model for a centrosymmetric hydrogen-bonded dimer that treats the high-frequency OH stretches harmonically and the low-frequency intermonomer (i.e. O···O) stretches anharmonically. This model takes into account the following effects: anharmonic coupling between the OH and O···O stretching modes; Davydov coupling between the two hydrogen bonds in the dimer; promotion of symmetry-forbidden OH stretching transitions; Fermi resonances between the fundamental of the OH stretches and the overtones of the in- and out-of-plane bending modes involving the OH groups; direct relaxation of the OH stretches; and indirect relaxation of the OH stretches via the O···O stretches. Using a set of physically significative parameters into this model, the authors reproduce the main features in the experimental OH(D) bands of these dimers. By increasing the number and strength of the Fermi resonances and by promoting symmetry-forbidden OH stretching transitions in our simulations, they directly see the emergence of the ABC structure, which is a characteristic feature in the spectra of very strongly hydrogen-bonded dimers. However, in the case of the deuterated dimers, which do not exhibit the ABC structure, the Fermi resonances are found to be much weaker.

The parameters corresponding to Figure 1.27 are given in Tables 1.21a and b.

1.3.2.11 Monomer of $(CH_3)_2O\cdots HCl$

Taking Into Account Coupling Between Slow and Bending Modes In a recent paper, Rekik et al. [33] have calculated the IR spectral density of the ν_S $(Cl-\vec{H})$ band in gaseous $(CH_3)_2O\cdots HCl$ complex in order to fit the experimental spectra obtained by Lassegues and Huong [37]. (See Figure 1.28) They have used a Morse curve for the potential of the slow mode and introduced an additional bending mode effect

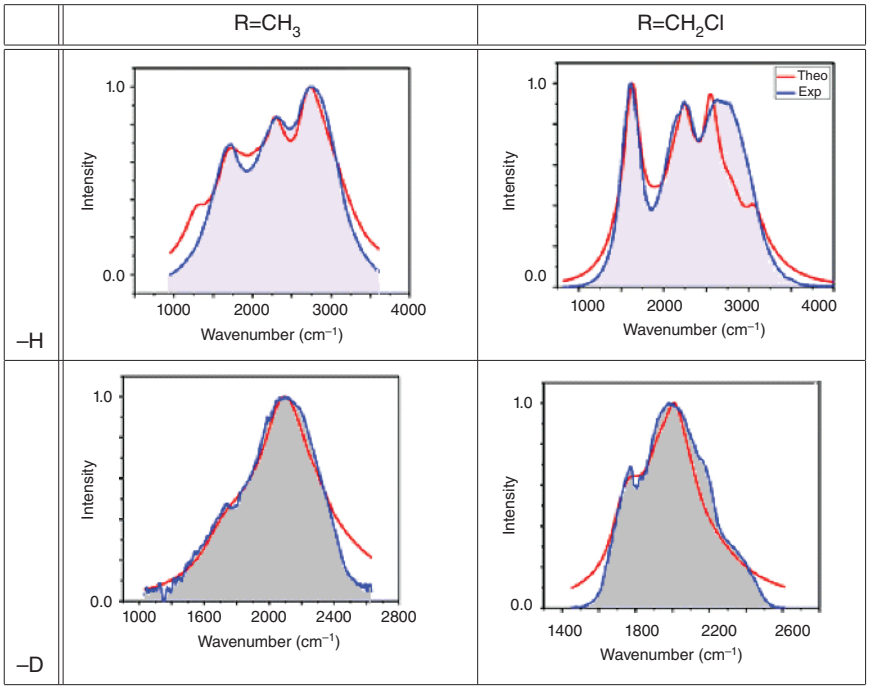

Figure 1.27 Comparison between experimental (grayed) and theoretical lineshapes of dimeric CH_3- and CH_2Cl- phosphinic acids H/D analogs. Source: Rekik et al. 2012 [33]/ American Chemical Society.

Table 1.21b Fermi resonance parameters for used for fitting the experimental lineshapes of $(CH_2Cl)_2PO_2H/D$ and $(CH_3)_2PO_2H/D$ (Continuation of Table 1.21a).

	$\Delta_1(cm^{-1})$	$\Delta_2(cm^{-1})$	$f_1(cm^{-1})$	$f_2(cm^{-1})$	$\gamma_1^{\delta}(\Omega)$	$\gamma_2^{\delta}(\Omega)$
$(CH_2Cl)_2PO_2H$	380	320	96	120	0.02	0.02
$(CH_2Cl)_2PO_2D$	225	115	30	10	0.02	0.02
$(CH_3)_2PO_2H$	−255	−220	110	120	0.02	0.02
$(CH_3)_2PO_2D$	5	25	15	20	0.02	0.02

for improving the fitting by the theoretical lineshape. This procedure writes the total Hamiltonian of the complex as the sum:the parameter $\alpha°$ and β are the coupling of the fast mode with respectively the slow and bending modes. They have compared their results with the experimental lineshape (grayed) with the parameters given in Table 1.22.

Taking Into Account Electrical Anharmonicity On the same compound, Rekik et al. [16, 17] take into account the electrical anharmonicity and dampings in explaining the IR spectrum of gaseous $(CH3)_2O\cdots HCl$ complex (see Figure 1.29 and corresponding data in Table 1.23).

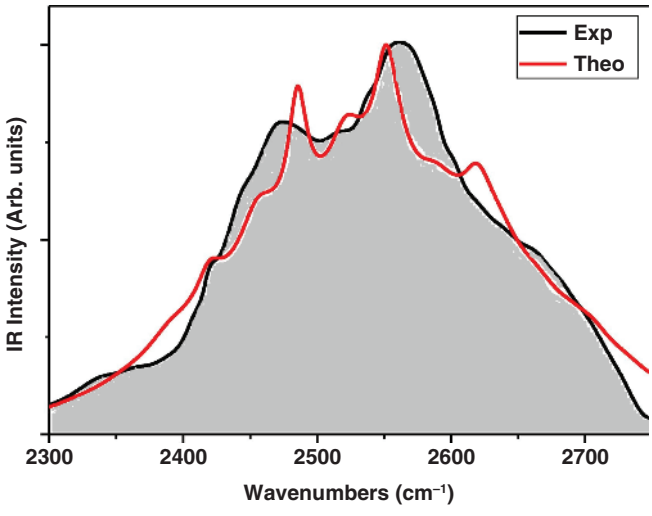

Figure 1.28 $(CH_3)_2$ O· · ·HCl complex in gas phase at 226 K . Source: Rekik et al. 2019 [34]/With permission of Elsevier.

Table 1.22 Parameters used in the theoretical lineshape of Figure 1.28.

$\omega°(cm^{-1})$	$\Omega(cm^{-1})$	$\alpha°$	β	$\Omega_\delta(cm^{-1})$	$\gamma°(\Omega)$	$\gamma_\delta(\Omega)$
2600	66	0.7985	0.3275	30	0.125	0.275

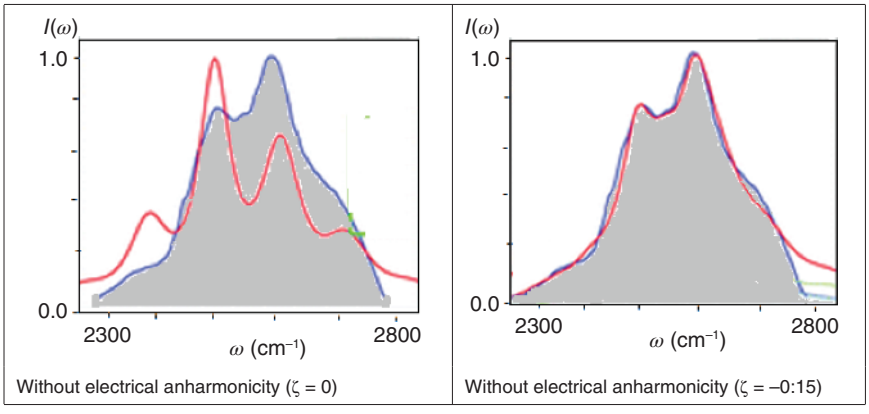

Figure 1.29 Gaseous $(CH_3)_2$ O· · ·HCl complex. Effect of the ζ electrical anharmonicity parameter. Source: Rekik et al. 2017 [17]/ Royal Society of Chemistry.

Table 1.23 Parameters used for fitting the lineshapes of gaseous $(CH3)_2O\cdots HCl$ complex.

	$\omega°(cm^{-1})$	$\Omega(cm^{-1})$	$\alpha°$	$\gamma°(\Omega)$	$\gamma(\Omega)$	ζ
$CH_3O^{\cdots}HCl$	2579	106	0.721	0.30	0.20	−0.15

They demonstrated the ability of a simple anharmonic model of the dipole moment function of the X–H stretching band to explain a set of spectroscopic features of hydrogen bonding formation.

1.4 Conclusion

In this chapter, before exposing the experimental tests of our theory of IR spectra of cyclic H-bonded dimers, we have given the main theoretical elements to allow its use, from the basic idea of an anharmonic coupling between a mode of low frequency and a mode of high frequency, through the introduction of various effects such as the Davydov effect, Fermi resonances or electrical anharmonicity.

The good results obtained for the adjustment of the experimental spectra by those who have systematically used this theory can find in this work a good recognition of their efforts towards a good understanding of the behavior of hydrogen bonds.

1.5 Acknowledgment

The authors are grateful to Ms. Joëlle Sulian for the preparation of several figures in this manuscript.

References

1 Blaise, P., Wójcik, M.J., and Henri-Rousseau, O. (2005). *J. Chem. Phys.* 122: 064306.
2 Maréchal, Y. and Witkowski, A. (1968). *J. Chem. Phys.* 48: 3637.
3 Boulil, B., Henri-Rousseau, O., and Blaise, P. (1988). *Chem. Phys.* 126: 263.
4 Rösch, N. and Ratner, M. (1974). *J. Chem. Phys.* 61: 3344.
5 Henri-Rousseau, O. and Blaise, P. (1998). The infrared spectral density of weak hydrogen bonds within the linear response theory. *Adv. Chem. Phys.*, vol. 103 (eds. I. Prigogine and S.A. Rice), 1–186. New York: Wiley.
6 Blaise, P., Déjardin, P.-M., and Henri-Rousseau, O. (2005). *Chem. Phys.* 313: 177.
7 Sakun, V. (1985). *Chem. Phys.* 99: 457.
8 Abramczyk, H. (1985). *Chem. Phys.* 94: 91.
9 Robertson, G. and Yarwood, J. (1978). *Chem. Phys.* 32: 267.
10 Bratos, S. and Hadzi, D. (1957). *J. Chem. Phys.* 27: 991.

11 Chamma, D. and Henri-Rousseau, O. (1999). *Chem. Phys.* 248: 91–104.
12 Witkowski, A. and Wojcik, M. (1973). *Chem. Phys.* 1: 9–16.
13 Davydov, A. (1962). *Theory of Molecular Excitons*. New York: McGraw Hill.
14 Rekik, N., Al-Agel, F.-A., and Flakus, H.-T. (2016). *Chem. Phys. Lett.* 647: 107–113.
15 Rekik, N. and Wójcik, M.J. (2010). *Chem. Phys.* 369: 71–81.
16 Rekik, N., Suleiman, J., Blaise, P. et al. (2017). *Phys. Chem. Chem. Phys.* 19: 5917–5931.
17 Rekik, N. and Alshammari, M.F. (2017). *Chem. Phys. Lett.* 678: 222–232.
18 Henri-Rousseau, O. and Blaise, P. (2008). *Adv. Chem. Phys.* 139 (5): 245–496.
19 Blaise, P., El-Amine Benmalti, M., and Henri-Rousseau, O. (2006). *J. Chem. Phys.* 124: 024514.
20 Haurie, M. and Novak, A. (1965). *J. Chim. Phys.* 62: 146.
21 Benmalti, M.E.-A., Blaise, P., Flakus, H.T., and Henri-Rousseau, O. (2006). *Chem. Phys.* 320: 267–274.
22 Bournay, J. and Maréchal, Y. (1971). *J. Chem. Phys.* 55: 1230.
23 Auvert, G. and Maréchal, Y. (1979). *Chem. Phys.* 40: 51; *ibid*, p. 61.
24 Flakus, H.T. and Miros, A. (1999). *J. Mol. Struct.* 484: 103.
25 Flakus, H.T. and Chelmecki, M. (2002). *Spectrochim. Acta, Part A* 58: 179.
26 Issaoui, N., Ghalla, H., and Oujia, B. (2013). *J. Appl. Spectrosc.* 80 (1): 14–24.
27 Ghalla, H., Rekik, N., Michta, A., Oujia, B., and Flakus, H.T. (2010). *Spectrochim. Acta, Part A* 75-1: 37–47.
28 Fathi, S., Blaise, P., Ceausu-Velcescu, A., and Nasr, S. (2017). *Chem. Phys.* 492: 12–22.
29 Ghalla, H., Issaoui, N., and Oujia, B. (2012). *Int. J. Quantum Chem.* 112: 1373–1383.
30 Flakus, H.T., Jabonska, M., and Kusz, J. (2009). *Vib. Spectrosc.* 49: 174.
31 Rekik, N., Flakus, H.T., Jarczyk-Jedryka, A. et al. (2015). *J. Phys. Chem. Solids* 77: 68–84.
32 Rekik, N., Ghalla, H., and Hanna, G. (2012). *J. Phys. Chem. A* 116: 4495–4509.
33 Rekik, N., Salman, S., Suleiman, J. et al. (2019). *Chem. Phys.* 519: 110–125.
34 Rekik, N., Flakus, H.T., Hachula, B. et al. (2020). *Spectrochim. Acta, Part A* 237: 118302.
35 Asfin, R.E., Denisov, G.S., and Tokhadze, K.G. (2002). *J. Mol. Struct.* 608: 161–168.
36 Rekik, N., Alsaif, N., Flakus, H.T. et al. (2020). *Spectrochim. Acta, Part A* 242: 118728.
37 Lassegues, J.C. and Huong, P.V. (1972). *Chem. Phys. Lett.* 17: 444–446.